Postprint of: Prześniak-Welenc M., Nadolska M., Nowak A., Sadowska K.: Pressure in charge. Neglected parameter in hydrothermal synthesis turns out to be crucial for electrochemical properties of ammonium vanadates ELECTROCHIMICA ACTA Vol. 339 (2020), 13591 DOI:10.1016/j.electacta.2020.135919

Pressure in charge. Neglected parameter in hydrothermal synthesis turns out to be crucial for electrochemical properties of ammonium vanadates

Marta Prześniak-Welenc[a*], *Małgorzata Nadolska*[a], *Andrzej P. Nowak*[b], *Kamila Sadowska*[a,1]

[a]Faculty of Applied Physics and Mathematics, Gdansk University of Technology, Narutowicza St. 11/12, 80-233 Gdansk, Poland

[b]Faculty of Chemistry, Gdansk University of Technology, Narutowicza St. 11/12, 80-233 Gdansk, Poland

* Corresponding author: e-mail: marta.welenc@pg.edu.pl, tell: +48 583486606, fax: +48 583471705

ABSTRACT: Ammonium vanadates are of great interest as they exhibit unusual electrical and sensory properties. $(NH_4)_2V_6O_{16}$ and $(NH_4)_2V_{10}O_{25}\cdot 8H_2O$ with various morphology were obtained in the hydrothermal synthesis under controlled temperature and pressure. It was shown, that the pure $(NH_4)_2V_{10}O_{25}\cdot 8H_2O$ was obtained under 50 bar of initial pressure, whereas lower pressure lead to the mixture of two compounds. The influence of the pressure was studied for the first time, and the results demonstrated its utmost importance. Moreover, the electrochemical performance of synthesized $(NH_4)_2V_{10}O_{25}\cdot 8H_2O$ was studied, revealing its excellent behavior as cathode material for Li-ion batteries. To the best of our knowledge, there is no information available on using this structure in such application.

KEYWORDS: Ammonium vanadate, solvothermal method, electrochemical characterization, Li-Ion battery

[1]Present address: Nalecz Institute of Biocybernetics and Biomedical Engineering, Polish Academy of Sciences. Ks. Trojdena St. 4; 02-109 Warsaw, Poland

1. INTRODUCTION

Ammonium vanadates are of great interest because of their structural diversity, rich chemistry and remarkable properties. Owing to the multivalence of vanadium, up to now, more than ten different forms with various stoichiometry have been investigated [1–9]. Moreover, ammonium vanadates are promising candidates for cathode material in lithium-ion batteries [10–14]. Some papers also report their usage as novel gas sensing material [15] or cathode material in multivalence-ion batteries [16–18]. The broad family of ammonium vanadates, with the general formula $(NH_4)_xV_yO_z$, are composed of vanadium oxide layers and NH_4^+ ions intercalated between them. The layered structure of vanadium oxides, with high theoretical charge storage capacity, can accommodate a large number of lithium ions. Furthermore, intercalated NH_4^+ ions increase the intrinsic conductivity and extend the interlayer spacing, improving the diffusion rate of lithium ions [19]. The embedded cations also stabilize the crystal structure (due to the presence of N–H···O hydrogen bonds), which is beneficial for the long-term cyclability of the electrode materials [20].

So far, many synthesis protocols have been reported leading to the formation of ammonium vanadates with diverse structures and morphologies [10],[21–26]. It is well-known, that both the structure and morphology of materials have a significant influence on their properties and consequently on their further utilization. Therefore, many efforts have been undertaken to control these features, mainly in order to enhance the electrochemical properties of ammonium vanadates. For example, nanostructures with large active surface areas shorten diffusion pathways and provide high charge capacity [24-25]. Recently, Liu et al. have obtained uniform mesoporous $NH_4V_4O_{10}$ nanoflowers which exhibited high capacity (242.8 mAh/g at a current density of 200 mA/g) and a long life cycle (65 % retention capacity after 200 cycles) [26]. Wang

et al. showed that $NH_4V_3O_8$ with a flower-like morphology deliver a maximum discharge capacity of 365 mAh/g at 15 mA/g with 84 % retention after 50 cycles [24]. In the literature, most syntheses are based on the facile hydrothermal method where an acidulated NH_4VO_3 solution is treated in a raised temperature (above 140°C) in a closed system. By varying the reaction time and temperature, various nanomaterials, such as $NH_4V_3O_8$ nanoflowers [24], $NH_4V_4O_{10}$ nanobelts or $(NH_4)_{0.6}V_2O_5$ square bricks [4] were obtained. In contrast, Zakharova at. al showed that these parameters affect only the size of the resulting particles - with increasing temperature and time particles decreased in size [27]. Indubitably, the acidity of the feed solution has a profound effect on the final hydrothermal product [28]. For instance, by changing the pH from 2.5 to 1.5 and then to 0.5, the obtained products were $NH_4V_4O_{10}$ nanobelts, $(NH_4)_2V_6O_{16}\cdot 1{,}5\ H_2O$ nanowires, $(NH_4)_6V_{10}O_{28}\cdot 6H_2O$ nanobundles, respectively [6]. It should be noticed that the pH value of the solution can be adjusted by various chemical reagents (such as, oxalic acid [2], [23-25], hydrochloric acid [6],[22] and others [27], [31-32]), which sometimes act also as forming agents. According to the literature, required structure growth can also be assisted by additional templating agents, e.g. sodium dodecyl benzene sulfonate [13], chitosan [33], and sodium carboxymethyl cellulose [34]. Although, synthesis protocols with different conditions (i.e. reaction time and temperature, pH of the growth solution, proper pH control compounds, surfactants and their molar ratio to the precursor) were thoroughly studied, the pressure effect has not yet been reported. Next to temperature, pressure is one of the most essential physical parameters required for hydrothermal conditions, and therefore its influence cannot be neglected in the synthesis.

To the best of our knowledge, presented in this paper $(NH_4)_2V_{10}O_{25}\cdot 8H_2O$ material has never been utilized as a cathode material for lithium-ion batteries. In the literature, one may find

information about the utilization of $(NH_4)_2V_{10}O_{25}\cdot 8H_2O$ for Zn-ion batteries [18] and in supercapacitors [8]. However, both examples describe the electrochemical performance of $(NH_4)_2V_{10}O_{25}\cdot 8H_2O$ in aqueous electrolyte. The specific capacity of such cathode material in the zinc-ion battery was equal to 229 mAh/g for a current density of 100 mA/g. However, it must be remembered that it is difficult to compare the results obtained in aqueous and non-aqueous electrolytes. In the case of aqueous systems, one should be aware of parasitic processes, which lead to loss of water, a decrease of energy, and continuous battery degradation. Such parasitic processes are not observed in non-aqueous systems consisted of one single cell. However, more than one cell is usually present in the battery. It may lead to the overcharge reactions and may become a considerable factor affecting battery performance.

In this work, the effect of the initial synthesis pressure on the ammonium vanadates phase and morphology have been studied for the first time. In the literature, the influence of temperature and pH on the obtained structures morphology and properties are frequently studied. However, there is a lack of study on the significance of the pressure during synthesis. Our results show, that this parameter cannot be neglected. As proof, we report the differences in the electrochemical behavior of samples synthesized under different initial pressures. It must be mentioned that comparing the results presented in the literature is difficult without the information of all synthesis parameters such as temperature, composition, pH, and pressure. Therefore, the studies about the influence of pressure are crucial in the development of the hydrothermal synthesis of ammonium vanadates and their further applications. Therefore, in this paper, samples have been prepared using a simple hydrothermal method without initial pressure and under 5, 25, and 50 bars. The resulting products were fully characterized by means of X-ray diffraction (XRD), scanning (SEM) and transmission electron microscopy (TEM), Fourier

transform infrared spectroscopy (FTIR) and thermogravimetric analysis (TG). Moreover, the electrochemical properties have been compared and assessed for application in lithium-ion battery**.**

2. EXPERIMENTAL

2.1 Material preparation

Ammonium metavanadate (NH_4VO_3, 99%) was purchased in Sigma Aldrich. Oxalic acid dihydrate ($C_2H_2O_4 \cdot 2H_2O$) was received from L.P P-H "OH". In all synthesis Mili-Q deionized water was used.

All samples were prepared *via* hydrothermal method in the autoclave. In a typical procedure, 0.250 g NH_4VO_3 and 0.250 g $C_2H_2O_4 \cdot 2H_2O$ were dissolved in 25 ml of deionised water under magnetic stirring. Then the obtained yellow solution (pH= 1) was placed into a stainless-steel autoclave with a capacity of 1800 ml and kept for 8 h at 180°C. After that time, the autoclave was evacuated with a rate of ca. 1 bar/min and then cooled to room temperature naturally. Finally, the obtained bluish-green precipitate was several times washed with deionised water and dried at 40°C under vacuum. In order to study the pressure effect, this procedure was repeated in pre-pressurized autoclave under 5, 25, or 50 bars. Required initial pressure was adjusted by filling the autoclave with N_2. Sample synthesised without initial pressure was denoted as p0 and samples obtained under initially set pressure were labelled as p5, p25, and p50, respectively.

2.2 Apparatus

X-ray diffraction patterns (XRD) were collected on a Philips X'PERT PLUS difractometer with Cu Kα radiation (λ = 1.5406 Å) and 2θ ranging from 5 to 70°. The FullProf Suite program was used to perform LeBail refinements using Thompson-Cox-Hastings pseudo-Voigt peak shapes.

The Fourier transform infrared (FTIR) spectra were recorded on Perkin Elmer Frontier spectrophotometer, with a resolution of 2 cm^{-1} in the range of 400–4000 cm^{-1}. In order to make measurements in transmittance mode, all samples were mixed with KBr and pressed to pellets. The surface morphology and fine grain structure of the samples were studied also at room temperature by a FEI Company Quanta FEG 250 scanning electron microscope (SEM) and a FEI TECNAI G2 F20 transition electron microscopy (TEM). Thermogravimetric analysis (TG) was carried out under argon atmosphere from 40°C to 560°C (with a heating rate 10°C/min) using Netzsch STA 449 F1. The first derivative of TGA, denoted as DTG, was calculated using Netzsch Proteus ThermalAnalysis program. The thermal behavior was also studied with mass spectrum (MS). The gases that come out from the samples during heating were monitored by the quadruple mass spectrometer Netzsch QMS 403 C Aëolos.

2.3 Electrochemical measurements.

The electrodes were prepared from a slurry containing 7:2:1 weight ratio of p0 or p50, carbon black as conducting agent and 10 wt% vinylidiene fluoride (PVDF) as a binder. After being blended in N-methylpyrrolidone, the slurry was spread on the thin aluminium foil. Next the discs were cut off dried under dynamic vacuum in an oven (Glass Oven B-595, Büchi, Germany) for 24 h at 60 °C. Dried disc electrodes were used in two-electrode Swagelok® cells with lithium foil as a counter and reference electrodes (99.9% purity, 0.75 mm thickness, AlfaAesar, USA), 1 M $LiPF_6$ in EC:DMC ratio 1:1 (LP30 Merck, Germany) as the electrolyte, and glass fibre (Schleicher & Schüll, Germany) as the separator. The battery tests of the samples were performed using the ATLAS 0961 MBI (Poland) multichannel battery testing system with different current densities. Cyclic voltammetry measurements (CV) were carried out on a

PGSTAT204 galvanostat/potentiostat over the potential range from 2.0 V to 4.0 V vs. Li/Li^+ with a scanning rate of 0.1 mV/s.

3. RESULTS AND DISCUSSION

3.1 Material characterization

The phase composition and crystallographic structure of the obtained samples were determined by XRD analysis (Figure 1). The XRD pattern of the sample p0 revealed, that it is composed of two phases $(NH_4)_2V_{10}O_{25}\cdot 8H_2O$ and $(NH_4)_2V_6O_{16}$, with the dominance of the first one. The presence of the $(NH_4)_2V_6O_{16}$ is revealed by its main diffraction peak located at 11.32° (star in Figure 1). The lattice parameters were determined from LeBail refinement (see ESI) and the obtained values are in good agreement with those reported in the literature [8], [18], [21]. Analysing the diffractograms of the samples p5, p25 and p50, it can be noticed, that the intensity of the diffraction peaks ascribed to $(NH_4)_2V_6O_{16}$ decreased as compared to p0 and was not observed in the case of p50, obtained under the highest initial pressure among studied. Generally, a higher pressure may lead to more homogenous solutions, assuring a comparable environment in the whole reaction mixture, which is beneficial for phase purity. It can also speed up the rate of a synthesis reaction, facilitating the reduction process. This suggests that $(NH_4)_2V_6O_{16}$ is an intermediate phase in the reaction and demonstrates that the phase structure of the final product is strongly dependent on the initial pressure of the reaction.

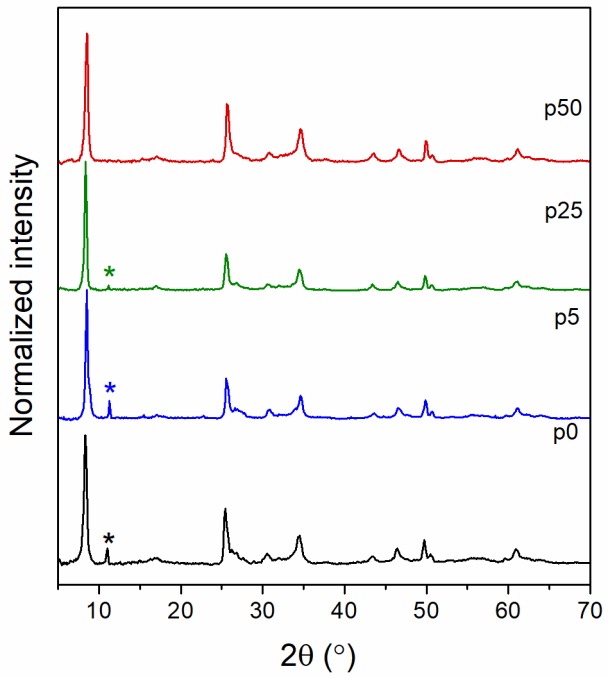

Figure 1. Normalized XRD patterns of p0, p5, p25 and p50.

Figure 2 shows the FTIR spectra of the obtained samples. Several distinct absorption bands appeared, which can be assigned to the different vibrational modes of N-H and V-O bonds. The absorption bands observed at ~3150 cm^{-1} and ~1400 cm^{-1} are due to the stretching and bending vibrations of the N-H in the NH_4^+ group. The sharp band centred at ~1000 cm^{-1} corresponds to V=O stretches. Bands present in the lower frequency region (765 cm^{-1} and 535 cm^{-1}) are characteristic for the symmetric and asymmetric stretching vibrations of the V-O-V bond. Furthermore, two bands at 3450 cm^{-1} and 1640 cm^{-1}, referring to the O–H stretching and bending vibration of the crystal water, confirmed the hydrated structure of analysed crystals [36]. Similarly to XRD results, the p0 revealed differences in spectroscopic data as compared to other samples. Splitting of bands arising from V-O (at 1000 cm^{-1}) and V-O-V (in the range 765 -500 cm^{-1}) observed in the p0 spectrum, indicates the presence of two inequivalent V=O groups [19].

According to the XRD results all samples exhibit two phases: the main one $(NH_4)_2V_{10}O_{25}\cdot 8H_2O$ and additional $(NH_4)_2V_6O_{16}$. The first one is composed of VO_5 square pyramids and the second one of VO_6 octahedrons, which differ in bond lengths and in consequence oscillate with different frequencies. Due to the fact that in the p0 sample contribution of the additional phase is the highest, the most distinct splitting of the bands is observed in the p0 spectrum.

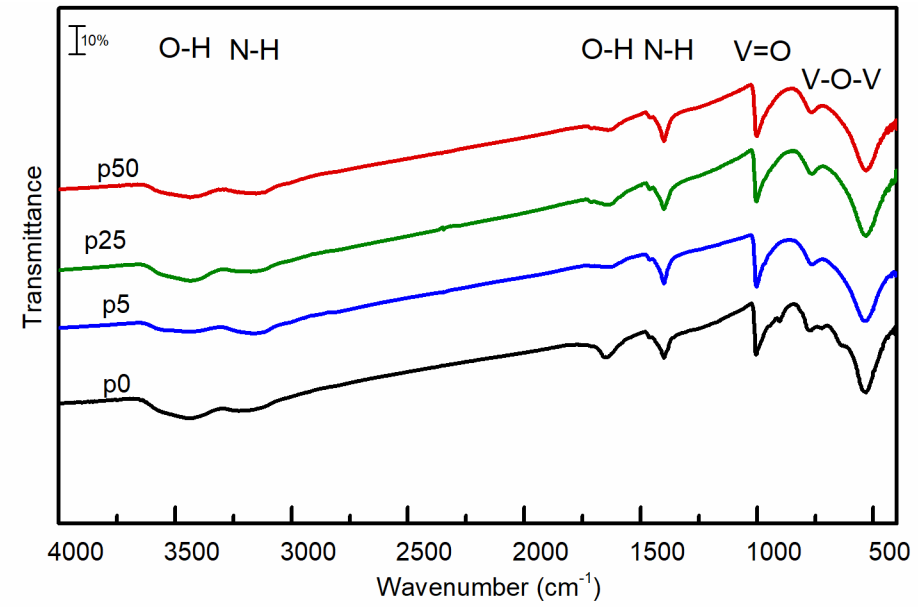

Figure 2. FTIR spectra of samples p0, p5, p25 and p50.

The morphology of the synthesized samples were investigated using SEM and TEM. As can be seen in Figure 3, different initial pressures in the hydrothermal synthesis lead to diverse samples morphologies. In the absence of the initial pressure the final product was the most heterogeneous- sample was a mixture of thick microplatelets as well as thin nanobelts. Moreover, microplatelets and nanobelts were randomly orientated and tended to agglomerate. In contrast, when the initial pressure was given, the obtained products were uniform and composed of only one kind of nanostructures. In addition, the nanostructures self-assemble into flower-like structures. It should be noticed here that usually to obtain such three-dimensional structures

additional soft or hard templates must be used [8], [11], [24]. In the case of sample obtained with 5 bars, flowers are built from nanoflakes with thickness up to 150 nm. Along with the further increase of the initial pressure nanoflakes elongate to thinner nanobelts. The obtained results show that initial synthesis pressure is a valuable tool for the synthesis of homogenous three-dimensional nanostructures.

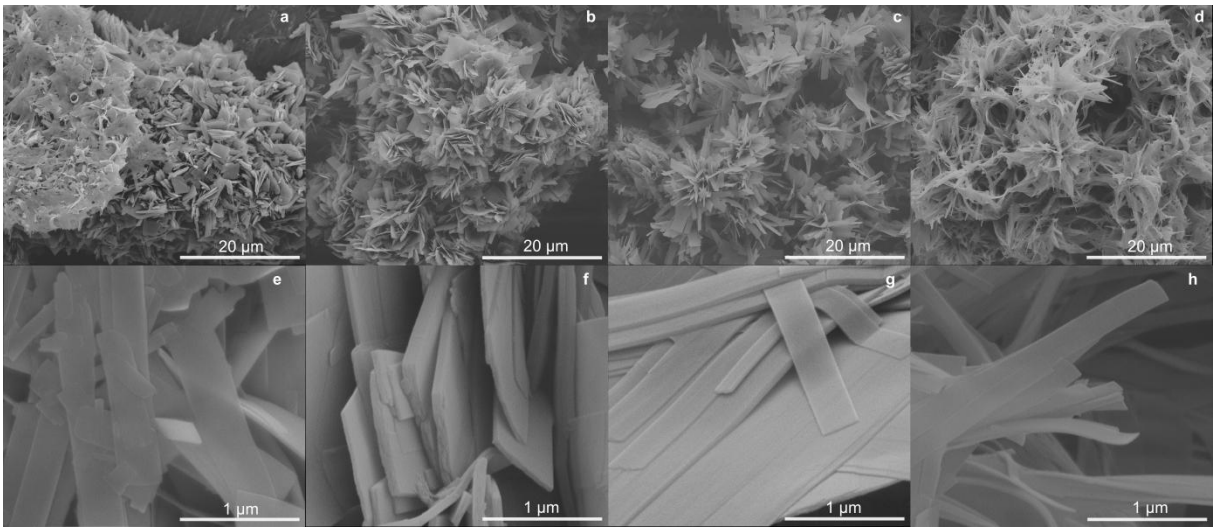

Figure 3. SEM images of samples p0 (a, e), p5 (b, f), p25 (c, g), p50 (d, h).

Further investigation using high-resolution TEM (HRTEM) and the corresponding selected-area electron diffraction pattern (SAED) revealed differences in the samples microstructure. A TEM and HRTEM images of the nanobelts obtained without initial pressure during synthesis (p0) are shown in Figure 4a and 4b respectively. It can be seen, that single nanobelt has poly-crystalline structure. White circles (Figure 4b), indicate areas of different lattice fringes orientations (inset in Figure 4b). It may be due to the fact that the p0 material is a mixture of two phases. According to XRD results, when the initial pressure increases to 50 bar, mostly phase $(NH_4)_2V_{10}O_{25}\cdot 8H_2O$ was obtained. Figure 4c shows a TEM image of typical nanobelt (sample p50) obtained at the highest pressure. The corresponding SAED pattern (inset of Figure 4c, black dot corresponds to the area where SAED pattern was recorded) exhibited very sharp diffraction

spots, indicating a single crystal structure of this nanostructure. The observed lattice spacing in the HRTEM image (Figure 4d) was calculated to be 0.344 nm and it matches well with the (003) plane of monoclinic $(NH_4)_2V_{10}O_{25}\cdot 8H_2O$.

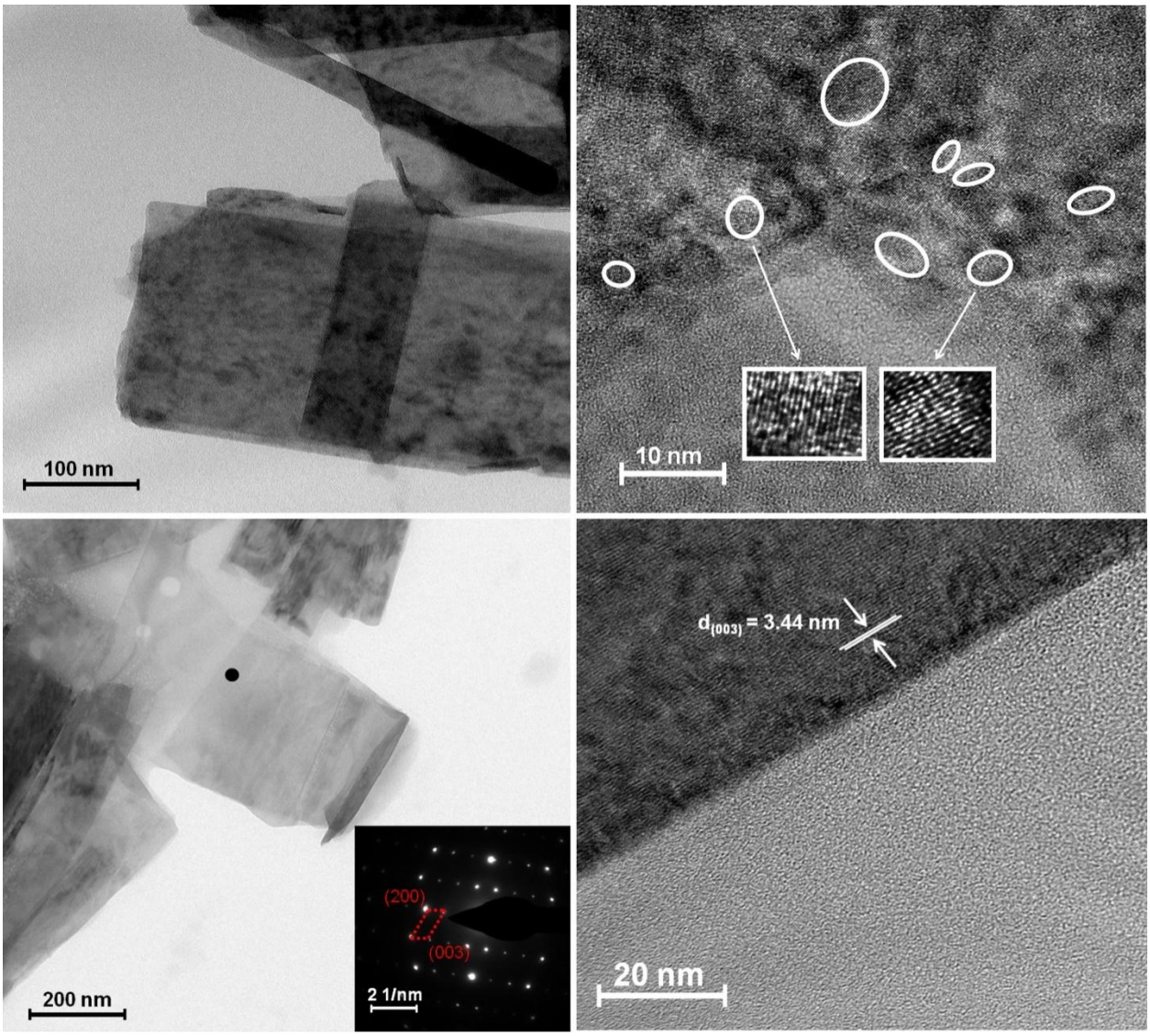

Figure 4. TEM (a,c) and HRTEM (b,d) images of samples p0 (a,b) and p50 (c,d). The inset in (c) is the SAED pattern.

In order to determine thermal stability of the obtained samples, thermogravimetric analysis (TG) with evolved gas analysis using mass spectrometry (MS) were performed. The mass spectra were measured from m/z 2 to 60. After the experiments, the measured peaks intensity were analyzed

as a function of the reaction time. The background of carrier gas was subtracted from m/z ion currents. The largest intensities of ion current were registered for the fragments corresponding to NH_3 and H_2O ions: *m/z* 14 (N^+), 15 (NH^+), 16 (NH_2^+, O^+) 17 (NH_3^+, OH^+), and 18 (H_2O^+). Figures 5a and 5b show TG and DTG (TG 1st derivative expressed in %/min, it determines rate of mass change) curves of p0 and p50 samples respectively with registered ion currents.

The thermal decomposition of measured samples occurred in three stages. From the TG/DTG plots, it is seen that the first thermal decomposition stage caused by the removal of the adsorbed water, occurred slightly in different temperature range for each sample. For sample p0 the first decomposition was observed between 40-205°C and for p50 in the range of 40-118°C, with a mass loss of 0.76% and 0.57%, respectively. The second weight loss of 7.22% between 205-362°C (with DTG peak at 336 °C) and 7.20% between 118-314°C (with DTG peak at 272°C) for p0 and p50 samples respectively was resulted mostly by the release of NH_3 and water formed as a result of the separation of the ammonium group. It is known that during the decomposition of vanadium ammonium compounds, equimolar amounts of NH_3 and H_2O are formed according to the equation:

$$n\ (NH_4)_xV_yO_z \rightarrow m\ (NH_4)_aV_bO_c + NH_3 + H_2O$$

For this reason, the curves presenting the ion current for m/z 18 (H_2O^+) and 15 (NH^+) are overlapping in this temperature range (Figure 5a and 5b). The last decomposition stage with mass loss of 3.16% (with DTG peak at 410°C) for p0 and 5.95% (with DTG peak at 340°C) for p50 was caused by the release of NH_3 and deintercalation of strongly-bounded water (the clearly visible shoulder on m/z 18 ion current). The visible differences in thermal stability result from phase composition, morphology, and microstructure of samples.

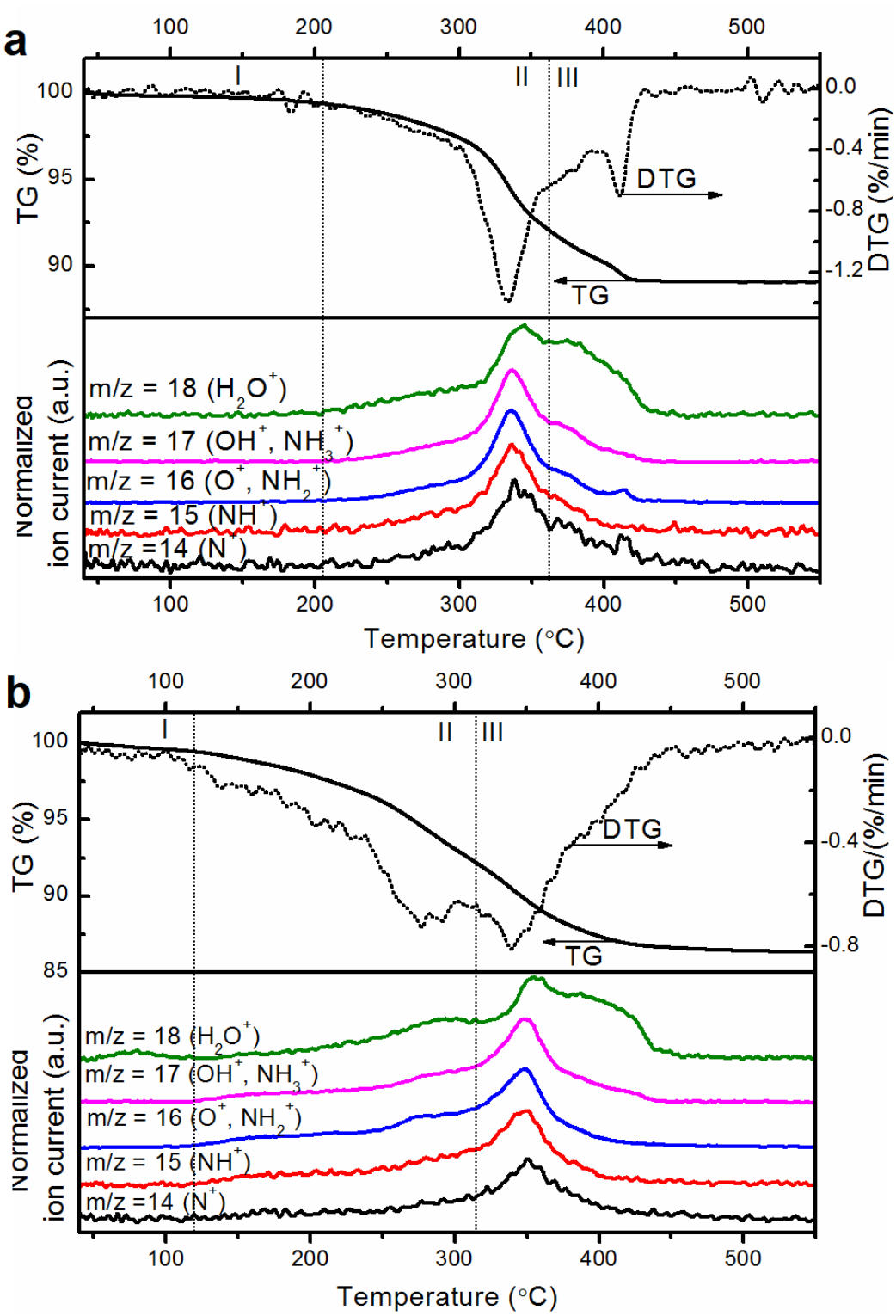

Figure 5. The TG and DTG curves of a) p0 and b) p50 sample with registered ion currents for NH_3 and H_2O ions in the evolved gas during the samples decomposition.

According to TEM and XRD results, sample p0 is composed of two phases ($(NH_4)_2V_6O_{16}$ and $(NH_4)_2V_{10}O_{25}\cdot 8H_2O$) and nanobelts have poly-crystalline structure (Figure 4b) and probably for this reason, the release of NH_3 occurs above 205°C. On the other hand, sample p50 consists of $(NH_4)_2V_{10}O_{25}\cdot 8H_2O$ phase and therefore weight loss associated with deintercalation strongly-bounded water (last decomposition stage) is almost twice as large.

3.2 Electrochemical performance

Ammonium vanadates are promising cathodic materials for Li-ion batteries. As it was mentioned before, $(NH_4)_2V_{10}O_{25}\cdot 8H_2O$ has not been studied in such application, so far. Figure 6 shows galvanostatic curves for 1st, 2nd, 3rd and 42nd charge/discharge cycle of p0 and p50 electrode material at 2 – 4 V at current density of 50 mA/g. The first discharge capacity for p0 and p50 recorded at 50 mA/g equals to 167 mAh/g and 261 mAh/g, respectively. The final specific capacity was 44 mAh/g and 229 mAh/g for p0 and p50, respectively. It gave capacity retention of 26 % for p0 and 87 % for p50. Thus, it is shown that p50 electrode material exhibits higher specific capacity with higher capacity retention in comparison with p0 material. The shape of the chronopotentiometric curve of p0 and p50 is similar.

One may see that the first three discharging cycles exhibit plateau at ~ 3.0 V, ~ 2.8 V and 2.5 V. In the reverse process one may see plateau at ~ 2.7 V. However, the shape of the curve for the 42nd cycle for p0 is totally different. It is very likely that material undergoes irreversible changes during lithium ion insertion/extraction process. The differences between p0 and p50 electrode material are well visible on the cyclic voltammetry curves in Figure 7. Both materials have two cathodic maxima at very close potentials, ~ 3.0 V (I) and 2.8 V (II). The third and fourth cathodic maxima are recorded at 2.61 V (III) and 2.52 V (III*) for p0, 2.56 V (III) and 2.44 V

(III*) for p50. These cathodic maximum are coupled with only one anodic current maximum at 2.66 V (iii) for p0 and 2.75 V (iii) for p50.

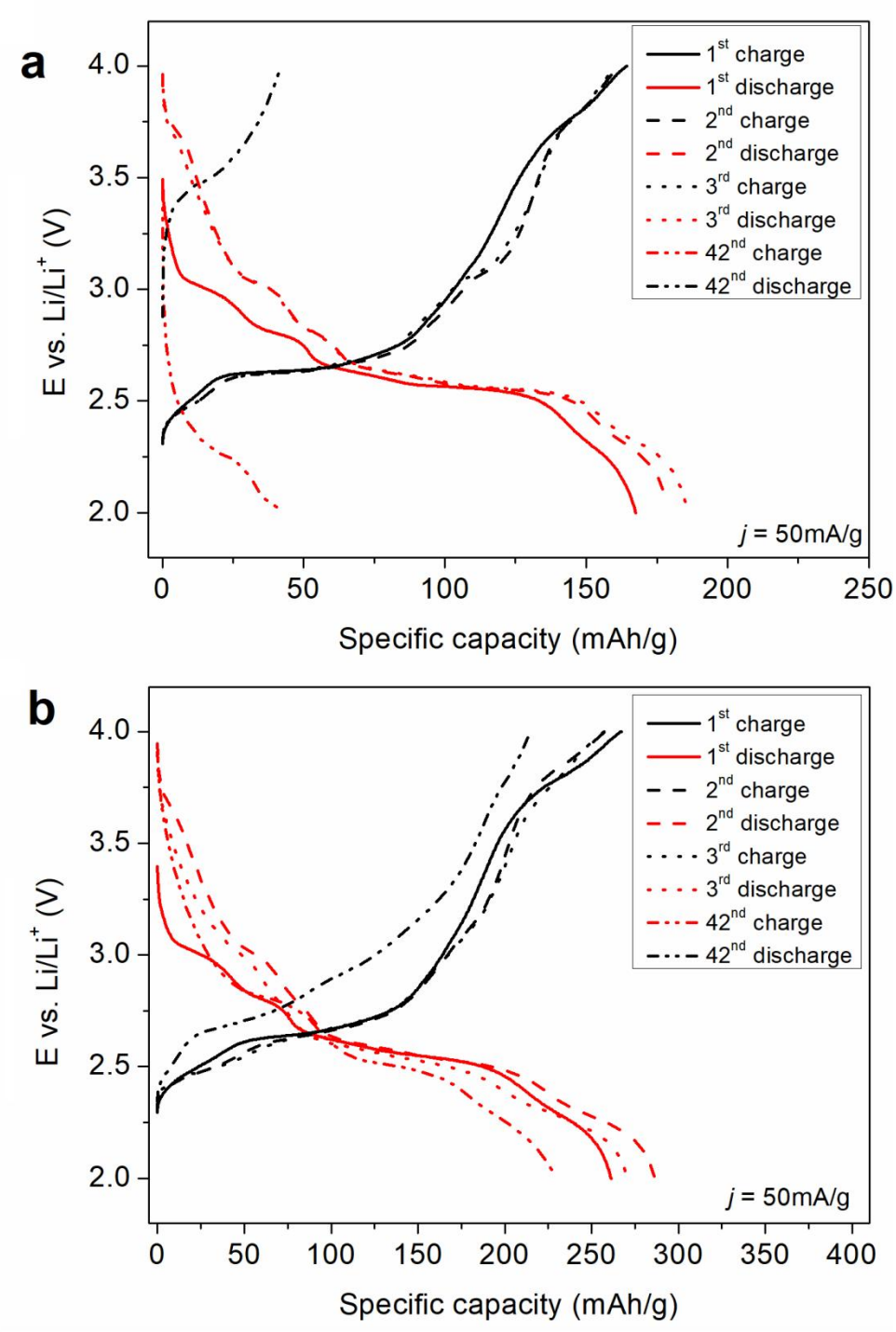

Figure 6. The first three and last 42 nd cycles of charge/discharge profiles of a) p0 and b) p50 electrode material.

We assume that the presence of two cathodic maxima is due to step reversible intercalation of lithium ions in the solid phase of both p0 and p50 electrode materials. Such phenomenon was observed for $NH_4V_3O_8 \cdot 0.2H_2O$ by Wang et. al. [3]. It is noteworthy to mention that the anodic maximum for p50 at 2.66 V (iii) hinders detection the anodic maximum at with 2.91 V (ii).

The p0 electrode material is a mixture consisting of $(NH_4)_2V_6O_{16}$ and $(NH_4)_2V_{10}O_{25} \cdot 8H_2O$ while the p50 is a pure $(NH_4)_2V_{10}O_{25} \cdot 8H_2O$ phase only. Further, the $(NH_4)_2V_{10}O_{25} \cdot 8H_2O$ is composed of double layer δ-MV_2O_5 type structure known in the literature as δ-$M_xV_4O_{10}$ [36]. Thus, in the studied case one may conclude that $(NH_4)_2V_{10}O_{25} \cdot 8H_2O$ is built of two molecules of $NH_4V_4O_{10} \cdot 4H_2O$ and one molecule of V_2O_5. The presence of water in $NH_4V_4O_{10} \cdot 4H_2O$ origins from the synthesis method. Hence, the difference in the composition of the electrode affects reaction with lithium ions regarding reversibility of Li^+ intercalation/deintercalation.

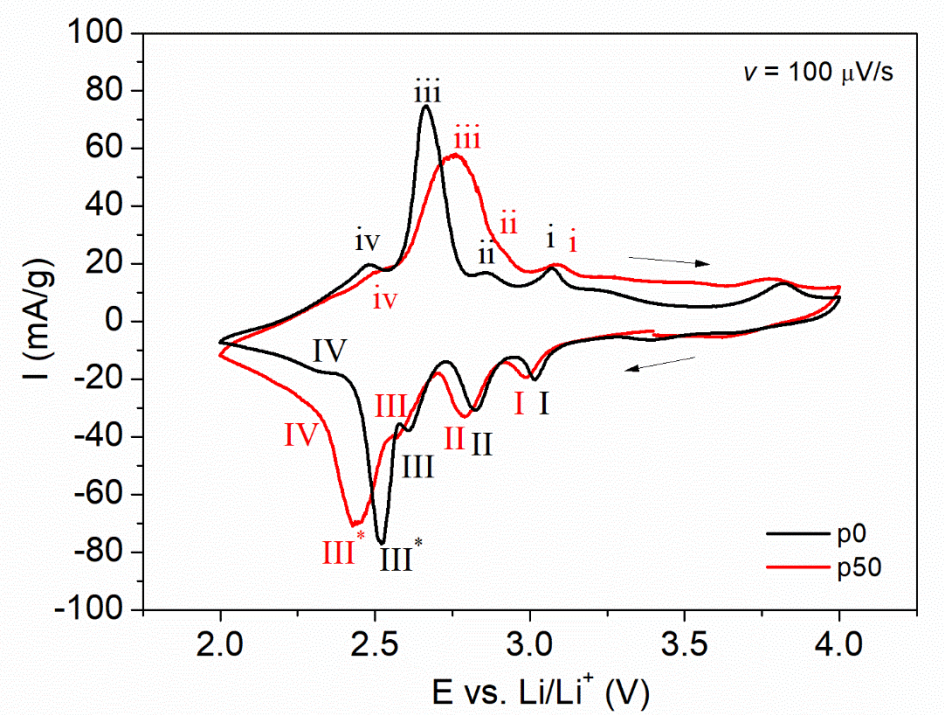

Figure 7. Cyclic voltammetry curves of the p0 and p50 electrode materials, scan 3.

The distance between the vanadium oxide layers in p50 seems to be more suitable for stabilization the structure during charging/discharging as it was already observed for lithium-rich layered materials [37-38]. It might be due to fact that $NH_4V_4O_{10}$ may inhibit lithium insertion between V_2O_5 layers of $(NH_4)_2V_{10}O_{25}\cdot 8H_2O$. Thus, the presence of three plateau during discharge (see Figure 6) and three cathodic maxima recorded on CV curve (see Figure 7) might be identified as lithium-ion intercalation process into ammonium vanadate structure according to equation [28,39]:

$$NH_4V_4O_{10} + (3\text{-}x)Li^+ + (3\text{-}x)e^- = Li_{3\text{-}x}NH_4V_4O_{10}$$

The theoretical capacity of $Li_{3\text{-}x}NH_4V_4O_{10}$ is of ~ 211 mAh/g. Taking into account the presence of two double layers of the $NH_4V_4O_{10}$ structure with V_2O_5 layer the theoretical amount of lithium ions able to be inserted into $(NH_4)_2V_{10}O_{25}\cdot 8H_2O$ is no less than 9 giving theoretical capacity at least 221 mAh/g. The rate performance of p0 and p50 electrode materials at varying current rates is shown in Figure 8. Electrode materials were tested in the sequence 50 mA/g → 100 mA/g → 150 mA/g → 200 mA/g → 150 mA/g →100 mA/g → 50 mA/g for six cycles in a sequence. The p0 electrode material exhibited stable electrochemical performance up to 12 cycles with specific charge and discharge capacities of 137 ± 7 mAh/g and 141 ± 2 mAh/g at 100 mA/g for the 12^{th} cycle, respectively. The 4 mAh/g difference in the specific capacity for charge/discharge process is due to open circuit potential (OCP) procedure applied between discharge and charge stages. During that time lithium ions migrate from host material to the electrolyte. Hence, for oxidation process less lithium ions can be extracted from an electrode material. The OCP procedure was applied to reach equilibrium state of the electrode material after discharging process.

The increase in current density to 150 mA/g caused capacity drop to 84 ± 10 mAh/g for the 18th discharge cycle. Even worse results were obtained for current density equal to 200 mA/g. The discharge capacity for the 24th cycle was 39 ± 6 mAh/g. It seemed that high current densities had an irreversible negative effect on the capacity of p0 electrode material. The p0 electrode material did not recover if the initial current density (50 mA/g) was applied. The discharge capacity for the 42nd cycle was only 49 ± 4 mAh/g. It is very likely that material underwent structural changes during applying high current density that did not allow lithium ions to be inserted into the host structure. The p0 electrode material seems to be inappropriate for lithium-ion storage because it possesses lower specific capacitance and is degrading during cycling. The additional intermediate phase $(NH_4)_2V_6O_{16}$, which is present in the p0 sample, is known to be suitable as cathode material for lithium-ion batteries. However, results showed that sample p0 had much lower capacity than values reported in the literature [24].

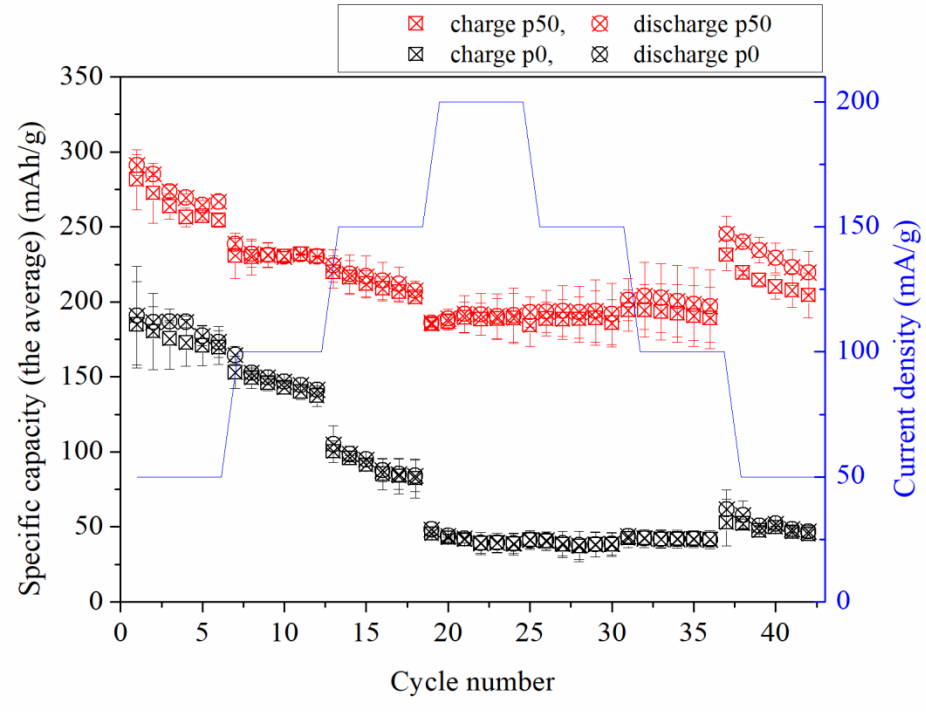

Figure 8. The rate capability of p0 and p50 electrodes in the potential range from 2.0 V to 4.0 V.

It should be noticed here that p0 is composed of two phases $(NH_4)_2V_{10}O_{25}•8H_2O$ and $(NH_4)_2V_6O_{16}$ with the dominance of the first one, and it cannot be treated as pure $(NH_4)_2V_6O_{16}$. It is suggested that in this case, the additional phase acts as a blocking agent for the lithium-ion insertion process. Moreover, it should not be forgotten that electrochemical performances of vanadium oxide-based materials are also strongly affected by the preparation method [40].

Much better results were obtained for p50 positive electrode material. One may see that during the continuous cycling with increasing and decreasing current densities, the specific capacity did not change significantly. The specific charge capacity at 50 mA/g was 254 ± 4 mAh/g and 204 ± 15 mAh/g for the 6^{th} and the 42^{nd} cycle, respectively. The specific discharge capacity was slightly higher with the values of 266 ± 5 mAh/g and 220 ± 14 mAh/g for the 6^{th} and the 42^{nd} cycle, respectively. It gives a capacity retention of 82.7 % for the discharge process.

During increase of current density one may see the capacity decrease. However, this decrease is not so drastic as it was observed for p0 electrode material. The discharge capacity for p50 for j = 200 mA/g was 191 ± 18 mAh/g, and did not change much when the current density increased to 100 mA/g (197 ± 24 mAh/g for the 36^{th} cycle). It shows that also for p50 high currents are very likely to change the crystallographic structure of p50. This change seems to be irreversible as the material did not reach values of specific capacities from the initial cycles. However, the high currents do not affect the specific capacity as much it was observed for p0 electrode material. In the all cases for p50 one may see capacity difference of about 10-15 mAh/g between charge and discharge process. This phenomenon is of the same origin as it was already described for p0 electrode material.

It is noteworthy that the specific discharge capacity for the 6^{th} cycle is 45 mAh/g higher in comparison with the theoretical capacity (221 mAh/g) which suggests that $(NH_4)_2V_{10}O_{25}·8H_2O$

structure can uptake more than 9 lithium ions during lithium insertion process. Moreover, the discharge capacity of 191 ± 18 mAh/g for j = 200 mA/g is only slightly lower than theoretical one. It can be concluded that p50 electrode material is a suitable for lithium-ion batteries.

4. CONCLUSIONS

Effect of the initial pressure on the final product was studied in the hydrothermal reaction of ammonium metavanadate and oxalic acid. The morphology and chemical structure of ammonium vanadates obtained with different initial pressure values (0, 5, 25, and 50 bar) were characterized by SEM, TEM, XRD, FTIR, TG and MS. Results indicate that the initial pressure affects both the morphology and the structure of the samples and cannot be omitted during the synthesis. It was found, that higher pressure results in more homogenous and thinner structures. Moreover, it facilities the formation of three-dimensional flower-like structures. It was also shown that the initial pressure is a key factor for the final phase composition of the samples. High pressure was necessary to obtain pure-phase $(NH_4)_2V_{10}O_{25}\cdot 8H_2O$. The electrochemical measurements revealed substantial differences between samples obtained under different pressure. The $(NH_4)_2V_{10}O_{25}\cdot 8H_2O$ was studied as a cathodic material for Li-ion batteries, showing great performance. The specific capacity of 191 mAh/g at 200 mA/g evidenced that the electrode material is stable during cycling at high current densities. This phenomenon is attributed to unique $(NH_4)_2V_{10}O_{25}\cdot 8H_2O$ structure that allows reversible lithium ion intercalation/deintercalation.

Author Contributions

The manuscript was written through contributions of all authors. All authors have given approval to the final version of the manuscript.

Funding Sources

Marta Prześniak-Welenc thanks National Science Centre, Poland for grant number 2017/01/X/ST5/01415. Kamila Sadowska (Żelechowska) thanks National Science Centre, Poland for grant number 2016/23/D/ST5/02800. Andrzej P. Nowak thanks Ministry of Science and Higher Education (DS no. 030893/ 003).

CRediT authorship contribution statement

Marta Prześniak-Welenc: Conceptualization, Supervision,Writing - original draft, Investigation, Funding acquisition. Małgorzata Nadolska: Writing - original draft, Investigation, Visualization. Andrzej P. Nowak: Writing - original draft, Investigation. Kamila Sadowska: Writing - original draft, Investigation, Funding acquisition.

REFERENCES

[1] G.S. Zakharova, I. V. Baklanova, A.Y. Suntsov, Y. Liu, Q. Zhu, W. Chen, $NH_4V_3O_7$: Synthesis, morphology, and optical properties, Russ. J. Inorg. Chem. 61 (2016) 1584–1590. https://doi.org/10.1134/S0036023616120214.

[2] G.Q. Zhang, S.T. Zhang, Charge-discharge mechanisms of ammonium vanadium bronze $NH_4V_4O_{10}$ nanobelts as cathode for lithium-ion battery, Asia-Pacific Power Energy Eng. Conf. APPEEC. 5 (2009) 2–5. https://doi.org/10.1109/APPEEC.2009.4918215.

[3] H. Wang, K. Huang, S. Liu, C. Huang, W. Wang, Y. Ren, Electrochemical property of $NH_4V_3O_8 \cdot 0.2H_2O$ flakes prepared by surfactant assisted hydrothermal method, J. Power Sources. 196 (2011) 788–792. https://doi.org/10.1016/j.jpowsour.2010.07.022.

[4] H. Fei, X. Wu, H. Li, M. Wei, Novel sodium intercalated $(NH_4)_2V_6O_{16}$ platelets: High performance cathode materials for lithium-ion battery, J. Colloid Interface Sci. 415 (2014) 85–88. https://doi.org/10.1016/j.jcis.2013.10.025.

[5] M.A. Teplonogova, A.D. Yapryntsev, A.E. Baranchikov, V.K. Ivanov, Selective hydrothermal synthesis of ammonium vanadates(V) and (IV,V), Transit. Met. Chem. (2018) 2–7. https://doi.org/10.1007/s11243-018-0265-x.

[6] N. Wang, W. Chen, L. Mai, Y. Dai, Selected-control hydrothermal synthesis and formation mechanism of 1D ammonium vanadate, J. Solid State Chem. 181 (2008) 652–657. https://doi.org/10.1016/j.jssc.2007.12.036.

[7] H.K. Park, G. Kim, Ammonium hexavanadate nanorods prepared by homogeneous precipitation using urea as cathodes for lithium batteries, Solid State Ionics. 181 (2010) 311–314. https://doi.org/10.1016/j.ssi.2010.01.011.

[8] Y. Jiang, L. Jiang, Z. Wu, P. Yang, H. Zhang, Z. Pan, et al., In situ growth of $(NH_4)_2V_{10}O_{25}\cdot 8H_2O$ urchin-like hierarchical arrays as superior electrodes for all-solid-state supercapacitors, J. Mater. Chem. A. 6 (2018) 16308–16315. https://doi.org/10.1039/c8ta05706k.

[9] T.Z. Ren, Z.Y. Yuan, X. Zou, Crystal growth of mixed-valence ammonium vanadates, Cryst. Res. Technol. 42 (2007) 317–320. https://doi.org/10.1002/crat.200610821.

[10] Y. Cheng, J. Huang, J. Li, L. Cao, Z. Xu, J. Wu, et al., Structure-controlled synthesis and electrochemical properties of $NH_4V_3O_8$ as cathode material for Lithium ion batteries, Electrochim. Acta. 212 (2016) 217–224. https://doi.org/10.1016/j.electacta.2016.07.008.

[11] D. Fang, Y. Cao, R. Liu, W. Xu, S. Liu, Z. Luo, et al., Novel hierarchical three-dimensional ammonium vanadate nanowires electrodes for lithium ion battery, Appl. Surf. Sci. 360 (2016) 658–665. https://doi.org/10.1016/j.apsusc.2015.11.038.

[12] Y. Ma, S. Ji, H. Zhou, S. Zhang, R. Li, J. Zhu, et al., Synthesis of novel ammonium vanadium bronze $(NH_4)_{0.6}V_2O_5$ and its application in Li-ion battery, RSC Adv. 5 (2015) 90888–90894. https://doi.org/10.1039/c5ra18074k.

[13] H. Wang, Y. Ren, W. Wang, X. Huang, K. Huang, Y. Wang, et al., $NH_4V_3O_8$ nanorod as a high performance cathode material for rechargeable Li-ion batteries, J. Power Sources. 199 (2012) 315–321. https://doi.org/10.1016/j.jpowsour.2011.10.069.

[14] H. Wang, K. Huang, C. Huang, S. Liu, Y. Ren, X. Huang, $(NH_4)_{0.5}V_2O_5$ nanobelt with good cycling stability as cathode material for Li-ion battery, J. Power Sources. 196 (2011) 5645–5650. https://doi.org/10.1016/j.jpowsour.2011.02.046.

[15] S.G. Leonardi, P. Primerano, N. Donato, G. Neri, Behavior of sheet-like crystalline ammonium trivanadate hemihydrate ($NH_4V_3O_8 \times 0.5H_2O$) as a novel ammonia sensing material, J. Solid State Chem. 202 (2013) 105–110. https://doi.org/10.1016/j.jssc.2013.03.028.

[16] E.A. Esparcia, M.S. Chae, J.D. Ocon, S.T. Hong, Ammonium Vanadium Bronze ($NH_4V_4O_{10}$) as a High-Capacity Cathode Material for Nonaqueous Magnesium-Ion Batteries, Chem. Mater. 30 (2018) 3690–3696. https://doi.org/10.1021/acs.chemmater.8b00462.

[17] T.N. Vo, H. Kim, J. Hur, W. Choi, I.T. Kim, Surfactant-assisted ammonium vanadium oxide as a superior cathode for calcium-ion batteries, J. Mater. Chem. A. 6 (2018) 22645–22654. https://doi.org/10.1039/C8TA07831A.

[18] C. Wang, T. Wei, Q. Li, G. Yang, Highly reversible and long-life cycling aqueous zinc-ion battery based on ultrathin $(NH_4)_2V_{10}O_{25}*8H_2O$ nanobelts, J. Mater. Chem. A. (2018). https://doi.org/10.1039/C8TA06626D.

[19] S.H. Lee, J.M. Koo, S.G. Oh, S.S. Im, Facile synthesis of ammonium vanadate nanofibers by using reflux in aqueous V_2O_5 solution with ammonium persulfate, Mater. Chem. Phys. 194 (2017) 313–321. https://doi.org/10.1016/j.matchemphys.2017.03.053.

[20] A. Ottmann, G.S. Zakharova, B. Ehrstein, R. Klingeler, Electrochemical performance of single crystal belt-like $NH_4V_3O_8$ as cathode material for lithium-ion batteries, Electrochim. Acta. 174 (2015) 682–687. https://doi.org/10.1016/j.electacta.2015.06.027.

[21] K.J. Range, C. Eglmeier, A.M. Heyns, D. Waal, Ammonium Hexavanadate, $(NH_4)_2V_6O_{16}$: Preparation, Crystal Structure, Infrared Spectra and High-Pressure Reactions, Zeitschrift fur Naturforsch. - Sect. B J. Chem. Sci. 45 (1990) 31–38. https://doi.org/10.1515/znb-1990-0108.

[22] D. Vernardou, M. Apostolopoulou, D. Louloudakis, N. Katsarakis, E. Koudoumas, Hydrothermal growth and characterization of shape-controlled $NH_4V_3O_8$, New J. Chem. 38 (2014) 2098–2104. https://doi.org/10.1039/c3nj01446k.

[23] H.K. Park, G. Kim, Ammonium hexavanadate nanorods prepared by homogeneous precipitation using urea as cathodes for lithium batteries, Solid State Ionics. 181 (2010) 311–314. https://doi.org/10.1016/j.ssi.2010.01.011.

[24] L. Kou, L. Cao, J. Huang, J. Yang, Y. Wang, Facile synthesis of $NH_4V_3O_8$ nanoflowers as advanced cathodes for high performance of lithium ion battery, J. Mater. Sci. Mater. Electron. 29 (2018) 4830–4834. https://doi.org/10.1007/s10854-017-8438-5.

[25] T.N. Vo, H. Kim, J. Hur, W. Choi, I.T. Kim, Surfactant-assisted ammonium vanadium oxide as a superior cathode for calcium-ion batteries, J. Mater. Chem. A. 6 (2018) 22645–22654. https://doi.org/10.1039/C8TA07831A.

[26] Y. Liu, M. Xu, B. Shen, Z. Xia, Y. Li, Y. Wu, et al., Facile synthesis of mesoporous $NH_4V_4O_{10}$ nanoflowers with high performance as cathode material for lithium battery, J. Mater. Sci. 53 (2018) 2045–2053. https://doi.org/10.1007/s10853-017-1619-z.

[27] G.S. Zakharova, C. Täschner, T. Kolb, C. Jähne, A. Leonhardt, B. Büchner, Morphology controlled $NH_4V_3O_8$ microcrystals by hydrothermal synthesis, Dalt. Trans. 42 (2013) 4897. https://doi.org/10.1039/c3dt32550d.

[28] S. Sarkar, P.S. Veluri, S. Mitra, Morphology controlled synthesis of layered $NH_4V_4O_{10}$ and the impact of binder on stable high rate electrochemical performance, Electrochim. Acta. 132 (2014) 448–456. https://doi.org/10.1016/j.electacta.2014.03.144.

[29] X. Tian, X. Xu, L. He, Q. Wei, M. Yan, L. Xu, et al., Ultrathin pre-lithiated V_6O_{13} nanosheet cathodes with enhanced electrical transport and cyclability, J. Power Sources. 255 (2014) 235–241. https://doi.org/10.1016/j.jpowsour.2014.01.017.

[30] K.F. Zhang, G.Q. Zhang, X. Liu, Z.X. Su, H.L. Li, Large scale hydrothermal synthesis and electrochemistry of ammonium vanadium bronze nanobelts, J. Power Sources. 157 (2006) 528–532. https://doi.org/10.1016/j.jpowsour.2005.07.043.

[31] G.S. Zakharova, A.P. Tyutyunnik, Q. Zhu, Y. Liu, W. Chen, Hydrothermal synthesis and thermal stability of self-assembling $NH_4V_3O_7$ microcrystals, Russ. J. Inorg. Chem. 60 (2015) 653–657. https://doi.org/10.1134/S0036023615060194.

[32] L. Liu, Q. Liu, W. Zhao, L. Wang, G. Li, L. Chen, Facile synthesis of $NH_4V_3O_8$ micro/nanoplates and the effects of cutoff potential on electrochemical performance, Int. J. Electrochem. Sci. 12 (2017) 11754–11762. https://doi.org/10.20964/2017.12.19.

[33] Y. Liu, B. Shen, X. Liu, Y. Wu, X. He, Q. Li, High-yield and eco-friendly fabrication of ultra-long $(NH_4)_2V_6O_{16}\cdot 1.5H_2O$ nanowires and their electrochemistry performances, Int. J. Electrochem. Sci. 12 (2017) 5483–5491. https://doi.org/10.20964/2017.06.31.

[34] H.A. Abbood, H. Peng, X. Gao, B. Tan, K. Huang, Fabrication of cross-like $NH_4V_4O_{10}$ nanobelt array controlled by CMC as soft template and photocatalytic activity of its calcinated product, Chem. Eng. J. 209 (2012) 245–254. https://doi.org/10.1016/j.cej.2012.08.027.

[35] S.G. Leonardi, P. Primerano, N. Donato, G. Neri, Behavior of sheet-like crystalline ammonium trivanadate hemihydrate ($NH_4V_3O_8\times 0.5H_2O$) as a novel ammonia sensing material, J. Solid State Chem. 202 (2013) 105–110. https://doi.org/10.1016/j.jssc.2013.03.028.

[36] P.Y. Zavalij, M.S. Whittingham, Structural chemistry of vanadium oxides with open frameworks, Acta Crystallogr. B. 55 (1999) 627–663. https://doi.org/10.1107/S0108768199004000.

[37] S. Taminato, M. Hirayama, K. Suzuki, K. Kim, Y. Zheng, K. Tamura, Mechanistic studies on lithium intercalation in a lithium-rich layered material using Li_2RuO_3 epitaxial film electrodes and in situ surface X-ray analysis, J. Mater. Chem. A. 2 (2014) 17875–17882. https://doi.org/10.1039/c4ta02795g.

[38] K. Ghatak, S. Basu, T. Das, V. Sharma, H. Kumar, D. Datta, Effect of cobalt content on the electrochemical properties and structural stability of NCA type cathode materials, Phys. Chem. Chem. Phys. 20 (2018) 22805–22817. https://doi.org/10.1039/c8cp03237h.

[39] C. Wang, H. Liu, M. Jiang, Y. Wang, R. Liu, Z. Luo, Applied Surface Science Ammonium vanadate@polypyrrole@manganese dioxide nanowire arrays with enhanced reversible lithium storage, Appl. Surf. Sci. 416 (2017) 402–410. https://doi.org/10.1016/j.apsusc.2017.04.069

[40] H.Y. Xu, H. Wang, Z.Q. Song, Y.W. Wang, H. Yan, M. Yoshimura, Novel chemical method for synthesis of LiV_3O_8 nanorods as cathode materials for lithium ion batteries Electrochim. Acta 49 (2004) 349–353. doi:10.1016/j.electacta.2003.08.017.

Supporting information

Pressure in charge. Neglected parameter in hydrothermal synthesis turns out to be crucial for electrochemical properties of ammonium vanadates

Marta Prześniak-Welenc[a*], Małgorzata Nadolska[a], Andrzej P. Nowak[b] and Kamila Sadowska[a]

[a]*Faculty of Applied Physics and Mathematics, Gdansk University of Technology, Narutowicza St. 11/12, 80-233 Gdansk, Poland*

[b]*Faculty of Chemistry, Gdansk University of Technology, Narutowicza St. 11/12, 80-233 Gdansk, Poland*

*Corresponding author; e-mail: marta.welenc@pg.edu.pl, tel: +48 583486606, fax: +48 583471705

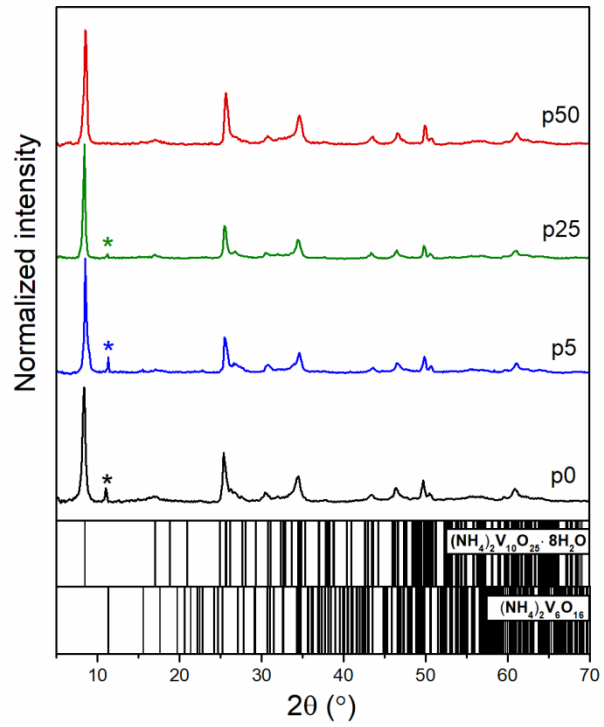

Fig. S1. Normalized XRD patterns of p0, p5, p25 and p50, with the theoretical Bragg peak positions for $(NH_4)_2V_{10}O_{25}\cdot 8H_2O$ and $(NH_4)_2V_6O_{16}$.

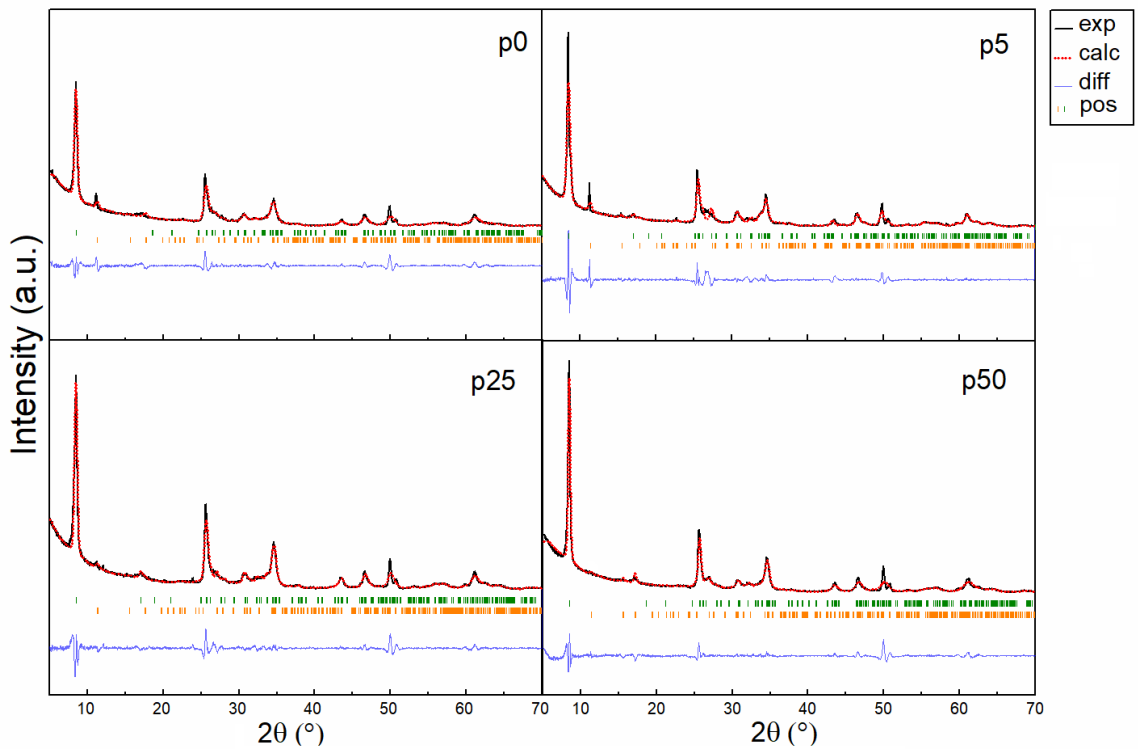

Fig. S2. Le Bail refinement of $(NH_4)_2V_{10}O_{25} \cdot 8H_2O$ and $(NH_4)_2V_6O_{16}$ for p0,p5,p25 and p50. The experimentally obtained data are shown with a black line, calculated pattern is shown with a red dots, the orange and green vertical marks indicate expected Bragg reflections for $(NH_4)_2V_{10}O_{25} \cdot 8H_2O$ and $(NH_4)_2V_6O_{16,}$ respectively. The blue line at the bottom shows the difference between the observed and calculated data

Phase 1: $(NH_4)_2V_{10}O_{25} \cdot 8H_2O$ (JCPDS 00-26-0097)

Phase 2: $(NH_4)_2V_6O_{16}$ (JCPDS 01-079-2051).

Tab. S1. The lattice parameters obtained from LeBail refinement

		a	b	c	α	β	γ
p0	phase 1	11,73	3,54	11,25	90	112,39	90
	phase 2	7,86	8,24	5,04	90	96,62	90
P5	phase 1	11,69	3,66	11,13	90	110,12	90
	phase 2	7,85	8,4	5,00	90	96,49	90
p25	phase 1	11,69	3,59	11,24	90	112,27	90
	phase 2	7,83	8,33	5,21	90	97,03	90
P50	phase 1	11,67	3,65	11,15	90	111,13	90
	phase 2	--	-	-	-	-	-